

Crystal structure analyses of uncomplexed ecotin in two crystal forms: Implications for its function and stability



DONG HAE SHIN,¹ HYUN KYU SONG,¹ IHN SIK SEONG,² CHEOL SOON LEE,²
CHIN HA CHUNG,² AND SE WON SUH¹

¹Department of Chemistry, Seoul National University, Seoul 151-742, Korea

²Department of Molecular Biology, Seoul National University, Seoul 151-742, Korea

(RECEIVED June 18, 1996; ACCEPTED August 22, 1996)

Abstract

Ecotin, a homodimeric protein composed of 142 residue subunits, is a novel serine protease inhibitor present in *Escherichia coli*. Its thermostability and acid stability, as well as broad specificity toward proteases, make it an interesting protein for structural characterization. Its structure in the uncomplexed state, determined for two different crystalline environments, allows a structural comparison of the free inhibitor with that in complex with trypsin. Although there is no gross structural rearrangement of ecotin when binding trypsin, the loops involved in binding trypsin show relatively large shifts in atomic positions. The inherent flexibility of the loops and the highly nonglobular shape are the two features essential for its inhibitory function. An insight into the understanding of the structural basis of thermostability and acid stability of ecotin is also provided by the present structure.

Keywords: ecotin; protease inhibitor; thermostability; X-ray structure

Serine protease inhibitors can be classified into various families on the basis of sequence similarity, topological similarity, and mechanism by which they bind their target proteases (Bode & Huber, 1991). For example, the substrate-like inhibitors, the serpin family inhibitors, and the hirudin-like inhibitors exhibit different modes of binding to and inhibiting serine proteases. Among them, the substrate-like inhibitors comprise relatively small proteins of 29–190 amino acid residues (Bode & Huber, 1992). They all possess an exposed binding loop of a characteristic canonical conformation. Most of the substrate-like inhibitors show rather narrow specificity toward the proteases. In contrast, ecotin inhibits a broad range of serine proteases with different substrate specificities (Chung et al., 1983).

Ecotin, a periplasmic serine protease inhibitor in *Escherichia coli*, consists of two identical subunits of 142 amino acid residues. Its molecular mass is 32,198 Da and its pI is 6.1. One dimeric inhibitor binds two protease molecules to form a tetrameric complex. Ecotin is an interesting inhibitor to study for several reasons. First, it is capable of inhibiting a broad range of serine proteases, including trypsin, chymotrypsin, elastase, rat mast cell chymase, and human plasma urokinase, as well as enzymes in the blood

coagulation cascade and other enzymes, such as kallikrein, fiddler crab collagenase, and granzyme B (Chung et al., 1983; Seymour et al., 1994; Tsu et al., 1994; McGrath et al., 1995). The reactive site of ecotin was determined to be Met 84 for its complexes with chymotrypsin, trypsin, porcine pancreatic elastase, factor Xa, factor XIIa, and plasma kallikrein (McGrath et al., 1991b; Seymour et al., 1994; Ulmer et al., 1995). Although the specificity of substrate-like canonical serine protease inhibitors is determined mostly by their P1 residue that fits into the binding pocket of the cognate protease, the P1 reactive site methionine residue of ecotin was proved not to be crucial for its specificity toward target proteases. The replacement of Met 84 with Ile, Arg, Glu, or Tyr showed little or no effect on the ability of ecotin to inhibit trypsin (Seong et al., 1994). Other interesting properties of ecotin are its exceptional thermostability and acid stability. Ecotin retained 94% of its inhibitory activity after heating for at least 30 min at 100 °C (Seong et al., 1994). Moreover, its activity was stable when exposed to pH 1.0 at 4 °C for 2 h (Chung et al., 1983).

Ecotin may play an important role in protecting the *E. coli* cells against exogenous proteases (Chung et al., 1983). In the mammalian gastrointestinal tract, which is the natural environment for *E. coli*, serine proteases such as trypsin, chymotrypsin, and elastase are present at high level. Therefore, one or more powerful inhibitors against these proteases would be essential for the survival of *E. coli* and ecotin is very well suited for this purpose.

Crystals of ecotin–trypsin complex (McGrath et al., 1991a), ecotin alone (Shin et al., 1993), and ecotin–crab collagenase complex (Tsu et al., 1994) have been reported. Also, the three-dimensional

Reprint requests to: Se Won Suh, Department of Chemistry, College of Natural Sciences, Seoul National University, Seoul 151-742, Korea; e-mail: sewonsuh@plaza.snu.ac.kr

Abbreviations: AOR, aldehyde ferredoxin oxidoreductase; BPTI, bovine pancreatic trypsin inhibitor; SSI, *Streptomyces* subtilisin inhibitor; SsIGPS, indole-3-glycerol phosphate synthase from *Sulfolobus solfataricus*.

structure of the ecotin–trypsin complex has been reported (McGrath et al., 1994). It reveals that Met 84 of ecotin is located on an extended surface loop, similar to the reactive site residue of other small serine protease inhibitors such as BPTI. However, the most striking feature is the presence of a second discrete and distal binding site for trypsin. This provides a model for a novel protein–protein interaction and for protease inhibition, because the protein dimerization is used to augment the binding energy and to allow chelation of the target protease.

In order to delineate the structural differences between uncomplexed and complexed ecotins, we report here the structure determination of the free inhibitor in two different crystal forms: the previously reported orthorhombic crystal (type I) (Shin et al., 1993) and a new, tetragonal crystal (type II), which diffracts to higher resolution than the former.

Results and discussion

Quality of the model

All residues are well defined by the electron density for the refined models of uncomplexed ecotin in both crystal forms (Fig. 1). This compares with the starting model of McGrath et al. (1994), in which six residues, 1–4 and 90–91, are missing. We have also modeled the correct side chains of eight residues (5, 9, 58, 65, 89, 92, 93, 103) that were built as alanines in the starting model of McGrath et al. (1994). *B*-factor plots against sequence number (subunit 1, residues 1–142; subunit 2, residues 501–642) are given in Figure 2. In both models of the uncomplexed ecotin, the loop around the P1 residue Met 84 and the N-terminal loop show *B*-factors higher than other regions. Table 1 summarizes the refinement statistics as well as model quality parameters. The mean positional error in atomic coordinates for both models is estimated to be within 0.3 Å by the Luzzati plot (Luzzati, 1952). Either β -octyl glucoside or trehalose was included in the crystallization conditions and many molecules of these additives could be located. Among 21 β -octyl glucoside molecules found in the asymmetric unit of type I crystal, one molecule lacks its octyl chain due to no electron density and six have only weak density for their octyl

chains. In addition, two have weak electron density for the glucose rings. All 18 trehalose (α -D-glucopyranosyl α -D-glucopyranoside) molecules in the asymmetric unit of type II crystal are well-defined by the electron density, except for five glucose rings, the discontinuous density of which was modeled as waters.

Overall structure

The overall fold of uncomplexed ecotin is equivalent to the previously reported structure of the inhibitor in complex with trypsin (McGrath et al., 1994). The most striking feature of ecotin is its nonglobular shape. In order to facilitate the following discussion on structural comparisons, some important features of the ecotin structure are reiterated briefly here. The ecotin dimer resembles a butterfly, with approximate dimensions of 70 Å \times 50 Å \times 20 Å. The monomer is a single domain composed of a mostly antiparallel seven-stranded β -barrel and loops connecting the secondary structure elements (Fig. 3; Kinemage 1). Ecotin lacks α -helices, but two 3_{10} -helices, formed by residues 6–10 and 101–106, are present in both complexed and uncomplexed inhibitor structures. One of these amphipathic 3_{10} -helices (G2) contributes to the formation of a hydrophobic core.

Three parts of ecotin are important for the inhibitory function: (1) the primary binding site, (2) the secondary binding site, and (3) the dimerization region. The P1 residue, Met 84, resides on a protruding loop, which is part of the primary binding site. For the residues P2–P1', the ecotin–trypsin structure and BPTI–trypsin structure (Perona et al., 1993a) were found to be essentially isostructural (McGrath et al., 1994). The primary binding site also contains a four-residue stretch (residues 51–54), through which ecotin makes additional contacts with trypsin. The two protruding loops containing these two interaction sites are linked by a disulfide bond between Cys 50 and Cys 87. The dimeric arrangement of ecotin allows it not only to bind trypsin at the active site through the above-mentioned primary binding region, but also to contact the protease using the secondary binding site provided by the other subunit. The secondary binding site comprises a loop containing residues 566–570 and neighboring residues 534, 608, and 610 of the other subunit. The long C-terminal tails from the two subunits

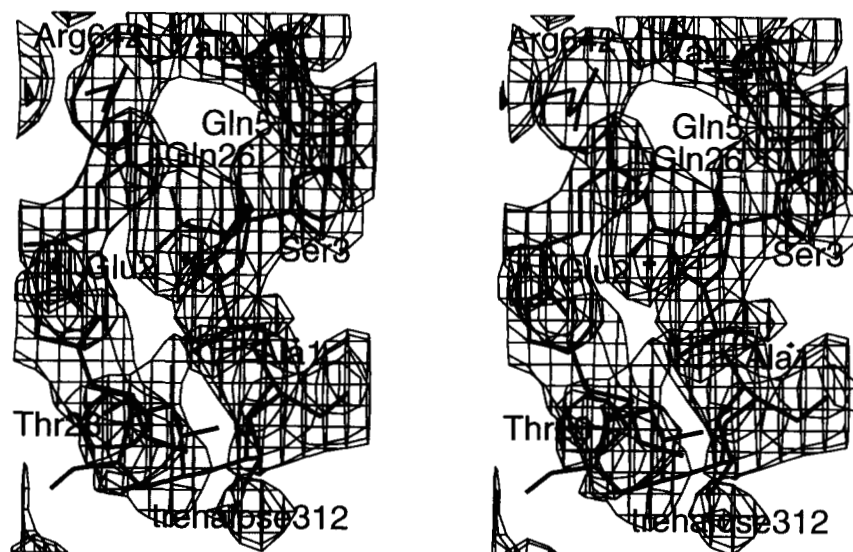


Fig. 1. Stereo diagram of final $2F_o - F_c$ map around the five N-terminal residues and one trehalose molecule in the tetragonal, type II crystal. The map is calculated with 20–2.19-Å data and contoured at 1.0σ . Figure was drawn using the program CHAIN (Sack, 1988).

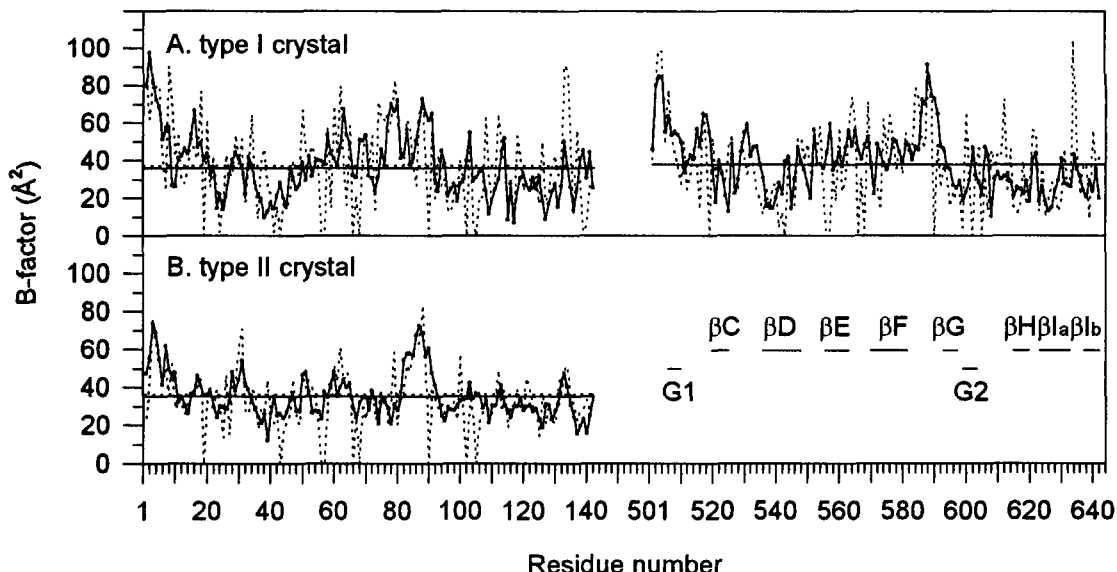


Fig. 2. *B*-factor plot of uncomplexed ecotin. (A) Type I and (B) type II crystals. Average *B*-factors for the main-chain atoms (solid lines) and side-chain atoms (dotted lines) are 37.6 \AA^2 and 38.4 \AA^2 (subunit 1 of type I crystal), 39.3 \AA^2 and 39.3 \AA^2 (subunit 2 of type I crystal), and 35.6 \AA^2 and 35.8 \AA^2 (type II crystal), respectively. Average values are indicated by horizontal lines. Assignment of secondary structural elements of uncomplexed ecotin is also given (β -strands: βC , residues 20–25; βD , 36–48; βE , 54–63; βF , 70–81; βG , 93–98; βH , 115–120; βIa , 124–132; βIb , 137–142; α_1 -helices: G1, 6–10; G2, 101–106).

form a two-stranded β -sheet. This association is mostly responsible for holding the monomers together in the dimer. Recently, domain swapping has been proposed as a possible mechanism for the evolution of multimeric proteins from monomers (Bennett et al., 1995). It is plausible that the present dimeric ecotin may have evolved from a monomeric inhibitor by domain swapping.

The additives, β -octyl glucoside or trehalose, play a role in the packing of ecotin molecules in two crystal lattices by weakly binding to the protein surface. The polar hydroxyl groups of β -octyl glucoside and trehalose interact with surface polar or charged residues of ecotin. Octyl chains of some β -octyl glucosides make van der Waals interactions with exposed hydrocarbon chains of arginine, lysine, or threonine residues. After it was shown by McPherson and his coworkers that the nonionic detergent β -octyl glucoside plays a beneficial role in crystallizing water-soluble proteins (McPherson et al., 1986), its inclusion as an additive in protein crystallization has become a routine practice. However, there have not been many reports of the bound detergent molecules in the refined structure. This study confirms the expectation that the bound detergent molecules shield the hydrophobic patches of atoms on the protein surface and thus reduce nonspecific interactions between protein molecules.

Structural comparisons among uncomplexed ecotins

Our present analyses of the structure of uncomplexed ecotin in two different crystal forms allow an evaluation of the flexibility of the inhibitor. Figure 4A shows the plot of RMS difference (RMSD) in atomic positions as a function of residue number for comparing ecotins in type I and II crystals. The RMSDs are 1.09 \AA for 1,136 main-chain atoms in the dimer and 1.63 \AA for 1,124 side-chain atoms, respectively. In contrast, those between the two independent monomers in type I crystal are 0.24 \AA for 568 main-chain atoms and 0.34 \AA for 562 side-chain atoms, respectively (Fig. 4B).

Large RMSDs in Figure 4A correspond to the loop around Met 84 (part of the primary binding site) and the N-terminal loop region, as well as the loop around residues 66–70 (part of the secondary binding site). This, along with high *B*-factors for the first two regions, indicates that these regions are the most flexible parts of the ecotin structure. Due to the inherent flexibility, their conformations are likely to be influenced by their interactions with the protease as well as the crystal packing environment, including the interactions with the bound additives such as β -octyl glucoside or trehalose.

Structural comparisons between uncomplexed and complexed ecotins

When the structure of ecotin in complex with trypsin is compared with those of the uncomplexed ecotins, the RMSD is either similar or slightly larger than when uncomplexed ecotins in two different crystal forms are compared. The RMSDs for comparing the structures of the complexed inhibitor and the free inhibitor in type I crystal are 1.04 \AA for 1,088 main-chain atoms in the dimer and 1.44 \AA for 1,032 side-chain atoms, respectively (Fig. 4C). Those for comparing the structures of the complexed inhibitor and the free inhibitor in type II crystal are 1.43 \AA and 1.92 \AA , respectively (Fig. 4D). Therefore, the complexed ecotin appears to be somewhat more similar to the uncomplexed ecotin in the orthorhombic, type I, crystal. Between type I and complexed, the loop around Met 84 (part of the primary binding site) shows the largest deviation, whereas between type II and complexed, not only this loop, but also the loop around residues 66–70 (part of the secondary binding site), show large deviations. This may be due partly to the involvement of the secondary binding loop in the crystal packing in type II crystal. A $C\alpha$ superposition of the free and complexed ecotins is given in Figure 5 (Kinemage 2). It shows a concerted shift of backbone atoms in the primary binding region of the in-

Table 1. Statistics for data collection and refinement for ecotin crystals

Crystal type	Orthorhombic (type I)		Tetragonal (type II)	
Data collection				
Number of crystals		1		1
Maximum resolution (Å)		2.68		2.19
Space group		P2 ₁ 2 ₁ 2 ₁		P4 ₃ 2 ₁ 2
Number of measured reflections		27,207		67,215
Number of unique reflections		7,810		8,537
<i>R</i> _{merge} ^a (%)		7.6		7.3
Completeness of data	Resolution range (Å)	Completeness (%)	Resolution range (Å)	Completeness (%)
	30.7–2.68	80.0	84.0–2.19	91.6
	2.80–2.68	25.2	2.29–2.19	73.2
Refinement				
Resolution range (Å)		6.0–2.68		6.0–2.19
No. of reflections (<i>F</i> > 2σ)		6,885		8,017
Completeness (%)		78.1		92.3
<i>R</i> -factor (%)		18.0		21.3
No. of non-hydrogen atoms				
Total		2,767		1,569
Protein (no. of residues)		2,260 (2 × 142)		1,130 (142)
Additive (no. of molecules)		412 (21 βOgs)		359 (18 trehaloses)
Water		95		80
Average <i>B</i> -factors (Å ²)	M1 (1–142)	M2 (501–642)		
Main-chain	37.6	39.3		35.6
Side-chain	38.4	39.3		35.8
Additive		54.2		58.7
Water		45.1		54.6
RMSD of geometry from ideal values				
Bond lengths (Å)		0.009		0.011
Bond angles (degrees)		1.552		1.819
Ramachandran outliers		0		0

^a*R*_{merge} = $\sum_h \sum_i |I(h)_i - \langle I(h) \rangle| / \sum_h \sum_i I(h)_i$, where *I*(*h*) is the intensity of reflection *h*, Σ_h is the sum over all reflections, and Σ_i is the sum over the *i* measurements of reflection *h*. *R*-factor = $\sum ||F_{\text{calc}}| - |F_{\text{obs}}|| / \sum |F_{\text{obs}}|$, where *F*_{calc} and *F*_{obs} are the calculated and observed structure factor amplitudes, respectively.

hibitor and its vicinity when in complex with trypsin. The nature of this structural change may be monitored by comparing the distances between Cα atom of Met 84 in the primary binding site and those of nearby residues (534, 566–570, 608, and 610) in the secondary binding site. The average of these distances is 21.5 Å, 23.6 Å, and 22.7 Å in complexed, type I, and type II crystals, respectively. Roughly speaking, therefore, the primary and secondary binding sites get closer to each other by 1–2 Å when trypsin binds to ecotin. Moreover, the distance between Cα atoms of Met 84 and Gly 102 is shortened by 2.5 Å in the complex with trypsin (Fig. 5).

Many of the side chains showing an RMSD exceeding the average value in a structural comparison between complexed and uncomplexed ecotins (Fig. 4C,D) are involved in trypsin binding and/or the crystal packing. The side-chain conformations worth mentioning are depicted in Figure 6. The side chain of P1 residue, Met 84, is more extended toward the cleft between the primary and secondary binding sites in the complexed structure than in the uncomplexed structure (Fig. 6A, Kinemage 3). The residues 51–54, forming the second contact region of the primary binding site, show similar side-chain conformations, except Leu 52 and Arg 54 (Fig. 6B). The side chains of residues 66–70 in the secondary binding site show similar conformations for both complexed ecotin

and uncomplexed inhibitor in type I crystal (Fig. 6C). However, those for the inhibitor in type II crystal show some differences, due to the close contact with neighboring molecules. The residues around 99–105, which contain part of the 3₁₀-helix (G2), also show large conformational differences on complexation (Fig. 6D).

The magnitude of structural changes in protease inhibitors when binding target enzymes ranges from very small to extremely large. For the best-characterized BPTI, the RMSD between complexed and uncomplexed inhibitors is 0.26–0.27 Å for 58 Cα atoms (Perona et al., 1993a). SSI exists as a dimer, with each monomer binding a protease molecule independently. The RMSD between 107 Cα atoms of free SSI and the inhibitor in SSI–subtilisin BPN' complex is 0.63 Å (Takeuchi et al., 1991). At the other extreme, the serine proteinase inhibitor (serpin) family shows the most dramatic conformational change. That is, the reactive site loop is inserted into a large central β-sheet after cleavage. A superposition of 54 Cα atoms in the central β-sheet of the uncleaved and cleaved α₁-antitrypsin gave an RMSD of 2.4 Å (Song et al., 1995). The RMSD between cleaved and uncleaved antithrombin III was 1.7 Å for a superposition of 61 Cα atoms (Schreuder et al., 1994). For ecotin, the RMSD between 136 Cα atoms in the uncomplexed and complexed inhibitor is 0.99 Å (for type I crystal) and 1.34 Å (for type II crystal). Ecotin resembles BPTI and SSI in that the primary

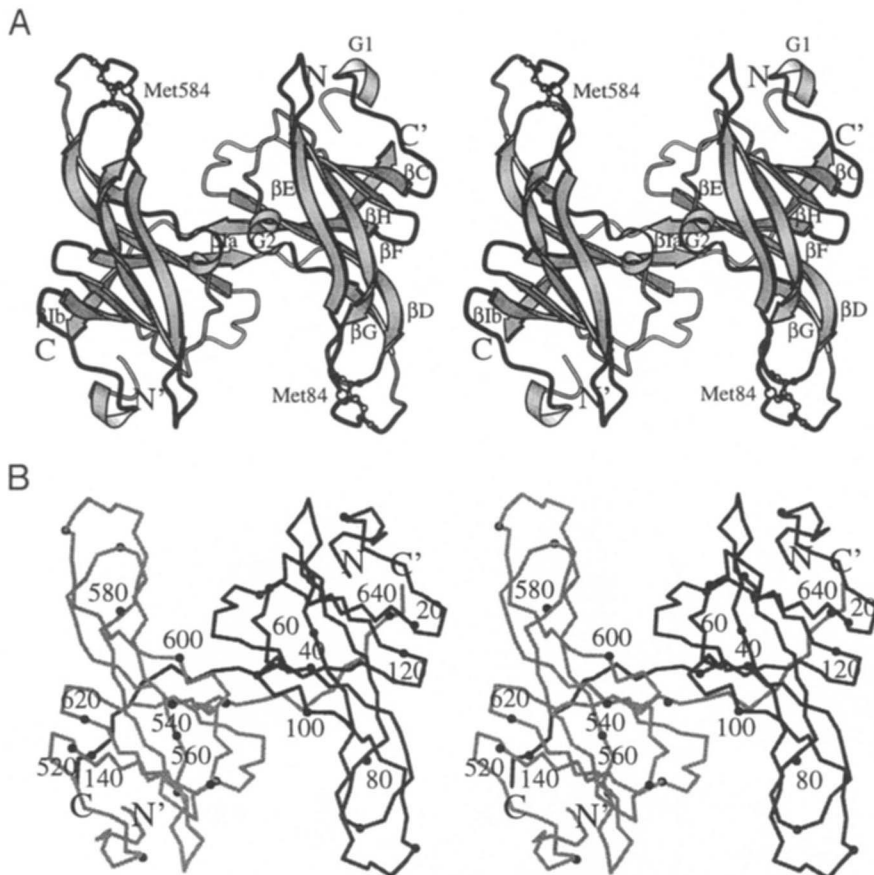


Fig. 3. **A:** Stereo ribbon diagram of ecotin. The N and C termini are indicated, as are the reactive P1 residue Met 84 and the disulfide bond between Cys 50 and Cys 87. Secondary structure was assigned with PROCHECK (Laskowski et al., 1993). Each subunit contains two α_{10} helices as well as seven β -strands. **B:** Stereo drawing of the $C\alpha$ trace of ecotin. Every tenth residue is represented by dot and every 20th residue is labeled. Figures drawn with MOLSCRIPT (Kraulis, 1991).

binding loop shows the most pronounced structural change when binding the target protease. Although the magnitude of the observed change for ecotin is larger than that for BPTI and SSI, the different resolutions and accuracies of the structures being compared have to be taken into account.

Altering the specificity toward target proteases

Ecotin inhibits many different serine proteases (Chung et al., 1983; McGrath et al., 1991b; Seymour et al., 1994; Ulmer et al., 1995). Figure 7 shows the sequence alignment of ten such target proteases: bovine chymotrypsin (BCHY), bovine trypsin (BTRYP), human plasma kallikrein (HKALL), human urokinase (HURO), factor XIIa (FXIIA), factor Xa (FXA), fiddler crab collagenase (FCCOL), granzyme B (GRAB), rat mast cell chymase (RMCC), and human leukocyte elastase (HLE). In the structure of ecotin–trypsin complex (McGrath et al., 1994), the primary binding site of ecotin interacts with the regions around the catalytic triad of trypsin (His 57, Asp 102, and Ser 195, according to the chymotrypsin sequence numbering scheme). The regions around these catalytic residues are highly conserved (Fig. 7). In addition, the secondary binding site of ecotin interacts with two segments of trypsin: one segment from residues 91 to 96, and the other from 237 to 240 (chymotrypsin numbering scheme will be followed for this discussion) (McGrath et al., 1994). The sequences around these two segments show limited homology (Fig. 7). The region of residues approximately from 160 to 180 is also likely to be important for binding ecotin, because the corresponding region in trypsin is in-

serted into the cleft between the primary and secondary binding sites of ecotin (McGrath et al., 1994). Three-dimensional structures of many serine proteases, including trypsin (Bode & Schwager, 1975), chymotrypsin (Blevins & Tulinsky, 1985), elastase (Bode et al., 1986), kallikrein (Bode et al., 1983), factor Xa (Padmanabhan et al., 1993), human factor D (Narayana et al., 1994), rat mast cell protease II (Remington et al., 1988), *Streptomyces griseus* trypsin-like protein (Read & James, 1988), and tonin (Fujinaga & James, 1987), share a common topology. Other proteases showing sequence similarity to these are expected to have a similar topology of folding. The dimeric ecotin appears to have evolved for an optimal inhibition of a broad range of serine proteases of similar topology. It is reasonable to anticipate that mutations of ecotin in the primary or secondary binding site may alter the specificity toward target proteases. In fact, mutants of ecotin in which the reactive Met 84 is replaced by arginine or lysine inhibit thrombin, factor XIa, activated protein C, and plasmin, which are not inhibited by the wild-type ecotin (Seymour et al., 1994).

Thermostability and acid stability of ecotin

Because no mesophilic homologue of ecotin is known, it is not possible to draw any firm conclusions about the structural origins of its exceptional thermostability through a structural or a sequence comparison. However, our refined models of uncomplexed ecotin in two different crystalline environments provide a useful insight into understanding the structural basis of its exceptional thermostability.

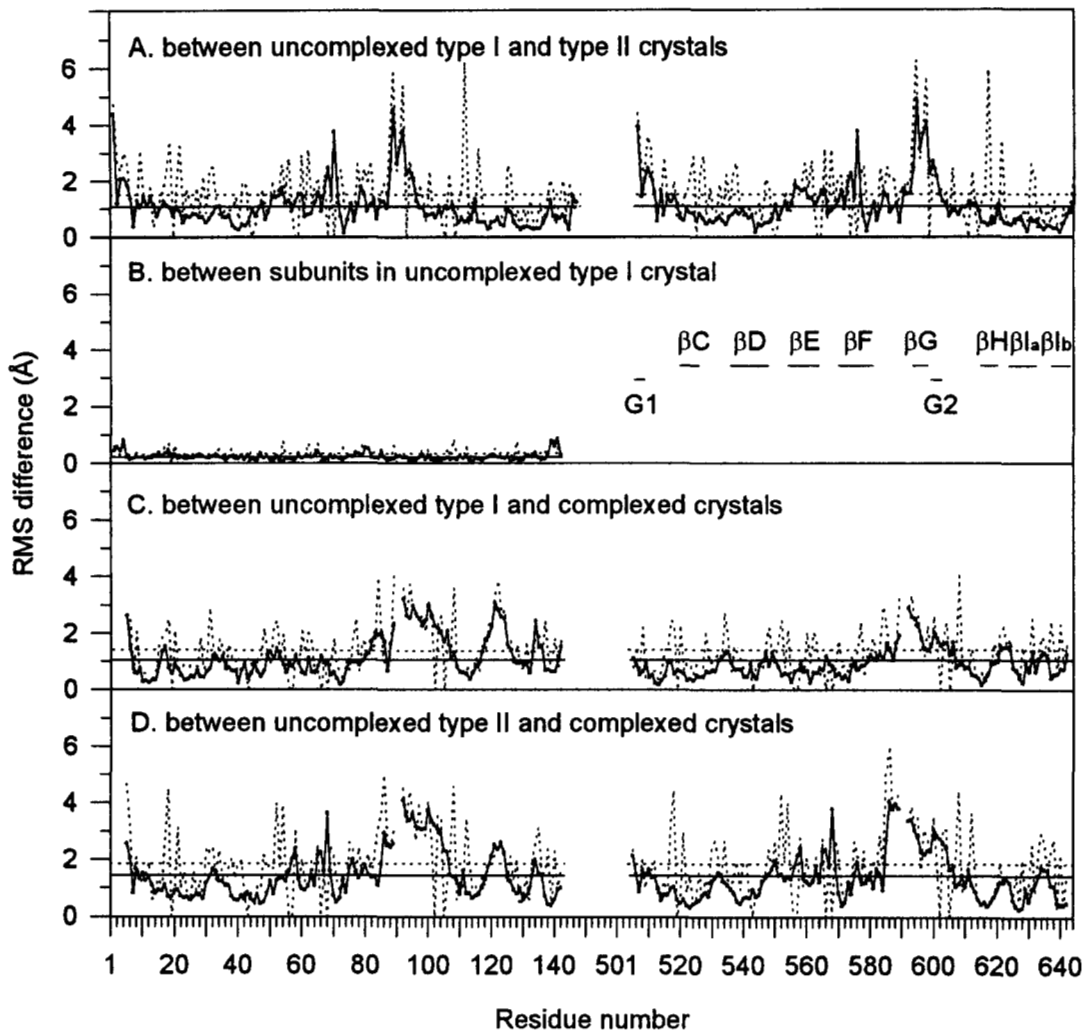


Fig. 4. RMSD plot for comparing ecotin structures. **A:** Between uncomplexed type I and type II crystals. **B:** Between subunits in uncomplexed type I crystal. **C:** Between uncomplexed type I crystal and ecotin complexed with trypsin. **D:** Between uncomplexed type II crystal and ecotin complexed with trypsin. RMSDs for main-chain atoms (solid lines) and side-chain atoms (dotted lines) of each residue are plotted. Average values are indicated by horizontal lines.

First, extremely thermostable proteins often lack a disulfide bond, let alone cysteine residues, and this may be due to the potential oxidation and degradation at this site (Lee et al., 1991b; Eom et al., 1995). However, very small proteins, not large enough to form a hydrophobic core, are usually stabilized by numerous disulfide bonds. The presence of a single disulfide bond in ecotin a few residues away from the reactive Met 84 in a flexible loop is intriguing. This is an intrasubunit disulfide bond between Cys 50 and Cys 87. This disulfide bond appears to play an important role in the maintenance of the structural stability rather than in the inhibitory activity. Supporting evidence comes from a mutagenesis experiment in which the replacement of Cys 87 with Ser showed no effect on the ability of ecotin to inhibit trypsin, chymotrypsin, or elastase. However, the C87S mutant ecotin was more sensitive to inactivation by heating at 100 °C than the wild-type inhibitor (Seong et al., 1994). The case of BPTI is similar in that the disulfide bond (Cys 14–Cys 38) in its protease binding loop may not be absolutely required for the inhibitory activity, but may be necessary for thermostability (Marks et al., 1987). In contrast, however, that of SSI, Cys 71–Cys 101, is critical to both inhibitory activity and thermo-

stability (Kojima et al., 1993). Because the disulfide bond is located on the protruding part of the ecotin structure, in the vicinity of the primary binding region and well separated from the main body of the protein, its role in protein stability may be limited to a local stabilization of this protruding part, which lacks a hydrophobic core of itself. A similar strengthening of solvent-exposed loops via salt bridges, instead of a disulfide bond, was proposed to be one of the contributing factors to the thermostability of indole-3-glycerol phosphate synthase from the hyperthermophile *Sulfolobus solfataricus* (Henning et al., 1995).

Second, salt bridges are found to be one of the major stabilizing forces for highly thermostable proteins. For example, for the hyperthermophilic tungstate oxidoreductase from *Pyrococcus furiosus*, the number of ion pairs per residue is more than twice the average (~0.085 versus ~0.04) (Chan et al., 1995). Ion pairs per residue was defined as the difference between the numbers of attractive and repulsive ionic interactions that occur between polar atoms of charged side chains within 4 Å, divided by the total number of residues (Barlow & Thornton, 1983; Chan et al., 1995). Similarly, for the hyperther-

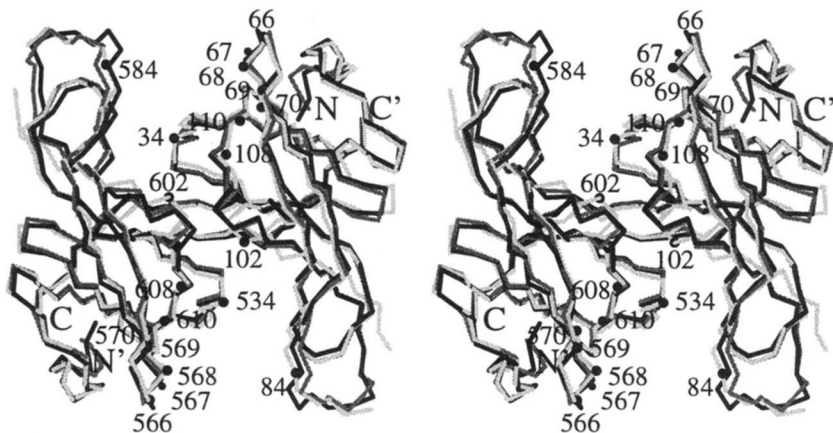


Fig. 5. Stereo diagram showing the superposition of $C\alpha$ atoms of ecotin structures. Ecotin complexed with trypsin (light lines), uncomplexed type I structure (grey lines), and uncomplexed type II structure (black lines). $C\alpha$ atoms of Met 84, Gly 102, and residues forming the secondary binding site are labeled.

mophilic enzyme glutamate dehydrogenase from *P. furiosus*, the number of ion pairs per residue (0.11) is approximately twice its mesophilic homologue (0.06) (Yip et al., 1995). Moreover, the distribution of the residues involved in ionic interactions in the hyperthermophilic enzymes shows a difference from the mesophilic ones. That is, in the hyperthermophilic enzymes, extensive ion pair networks or ion clusters were observed (Yip et al., 1995). In the case of free ecotin, the number of ion pairs per residue is either 0.060 (eight in one subunit and nine in the other) for the structure in type I crystal or 0.049 (seven per subunit) for type II, not much different from the average for mesophilic proteins. The distribution of residues involved in the salt bridges is not particularly unusual and there is no network of ion pairs (Fig. 8). Therefore, it may be concluded that the role played by salt bridges in the exceptional thermostability of ecotin cannot be a major one. This is consistent with the observation that more than half of the seven to nine ion pairs per ecotin monomer in the two different crystalline environments are not conserved, even if the distance limit for counting ion pairs is relaxed to 4.5 Å. One of the well-conserved ion pairs is between Glu 2 and Arg 642 (belonging to the other subunit) (Figs. 1, 8). The other is between the Glu 8 and Arg 22 (Fig. 8). The former salt bridge appears to contribute to the stabilization of both N and C termini and the latter to further stabilization of the N-terminal loop. Therefore, salt bridges may play at least a limited role in the thermostability of ecotin, if not a major role. Strengthening of polypeptide chain termini was also observed for the hyperthermophilic enzyme SsIGPS (Henning et al., 1995) and the reduction of flexibility in the termini of the polypeptide chain was proposed to be a contributing factor for thermostability (Politz et al., 1993). Our experience stresses the importance of comparing the structures in different crystalline environments for a meaningful assessment of the role of ion pairs in protein thermostability, because the side-chain conformations of charged residues involved in such ion pairs could be influenced significantly by the crystal environment.

Third, deamidation of asparagine residues was found to be one of the processes leading to the heat inactivation (Ahern & Klibanov, 1985). The formation of the major product of deamidation, isoaspartate, occurs frequently at Asn–Gly, Asn–Ser, or Asp–Gly sequences when they lie in regions of the polypeptide that are highly flexible (Aswad, 1990). Ecotin has two potential sites of deamidation and subsequent isoaspartate formation: Asp 89–Gly 90 and Asn 110–Ser 111. The former is located in a flexible loop belonging to the primary binding site. Two residues, Gly 90

and Lys 91, are missing from the structure of ecotin–trypsin complex determined by McGrath et al. (1994). This could result from either the isoaspartate formation and subsequent degradation at this site or from the disorder due to high flexibility. The latter possibility is more likely, because this part of the chain shows high *B*-factors in our models. In contrast, the sequence Asn 110–Ser 111 has low *B*-factors in both of our models and thus the region containing this sequence does not seem to be highly flexible. The electron density in our study indicates that an isoaspartate formation at the above two potential sites does not occur to any detectable level. It may be concluded that ecotin is resistant to thermoinactivation through deamidation and isoaspartate formation, even with the above two potential degradation sites.

Fourth, shorter loops may afford proteins some resistance to thermal unfolding, as in thermostable citrate synthase from *Thermoplasma acidophilum* (Russell et al., 1994). In the case of thermostable oligo-1,6-glucosidase from *Bacillus thermoglucosidasius* KP1006, proline residues occurring with high frequency in the loop regions were assumed to be responsible for the enhanced thermostability. The contents of proline residues in thermostable *B. cereus* oligo-1,6-glucosidase and thermostable oligo-1,6-glucosidase from *B. thermoglucosidasius* KP1006 are 19 of 558 residues (3.4%) and 33 of 562 residues (5.9%), respectively. That in ecotin is 8 of 142 residues (5.6%). Except for Pro 80, which belongs to a β -sheet, all other prolines are located within or close to the loop regions. The loop region containing Pro 88, which is part of the primary binding site and therefore interacts with trypsin in the complex structure (McGrath et al., 1994), extends toward the solvent. Other loops containing prolines are much shorter and do not extend much into the solvent. Therefore, the stabilization of loops by prolines is one of the factors responsible for the exceptional thermostability of ecotin.

Fifth, it is plausible that a reduced surface area and optimized packing of the atoms in the core of a structure increases protein stability. In the case of the extremely thermostable AOR, the accessible surface area is much reduced (Chan et al., 1995), as the low ratio of Ao/Ac indicates, where Ao and Ac are the observed and calculated surface areas. For the free ecotin, the ratio is 1.30 (in type I crystal) and 1.33 (in type II crystal). This unusually high ratio is not unexpected, because ecotin has a highly nonglobular shape. Therefore, the thermostability of ecotin cannot originate from the reduced surface area. Likewise, thermostability was not correlated with a reduced accessible surface area for SsIGPS (Henning et al., 1995). A simple indicator for evaluating the efficiency

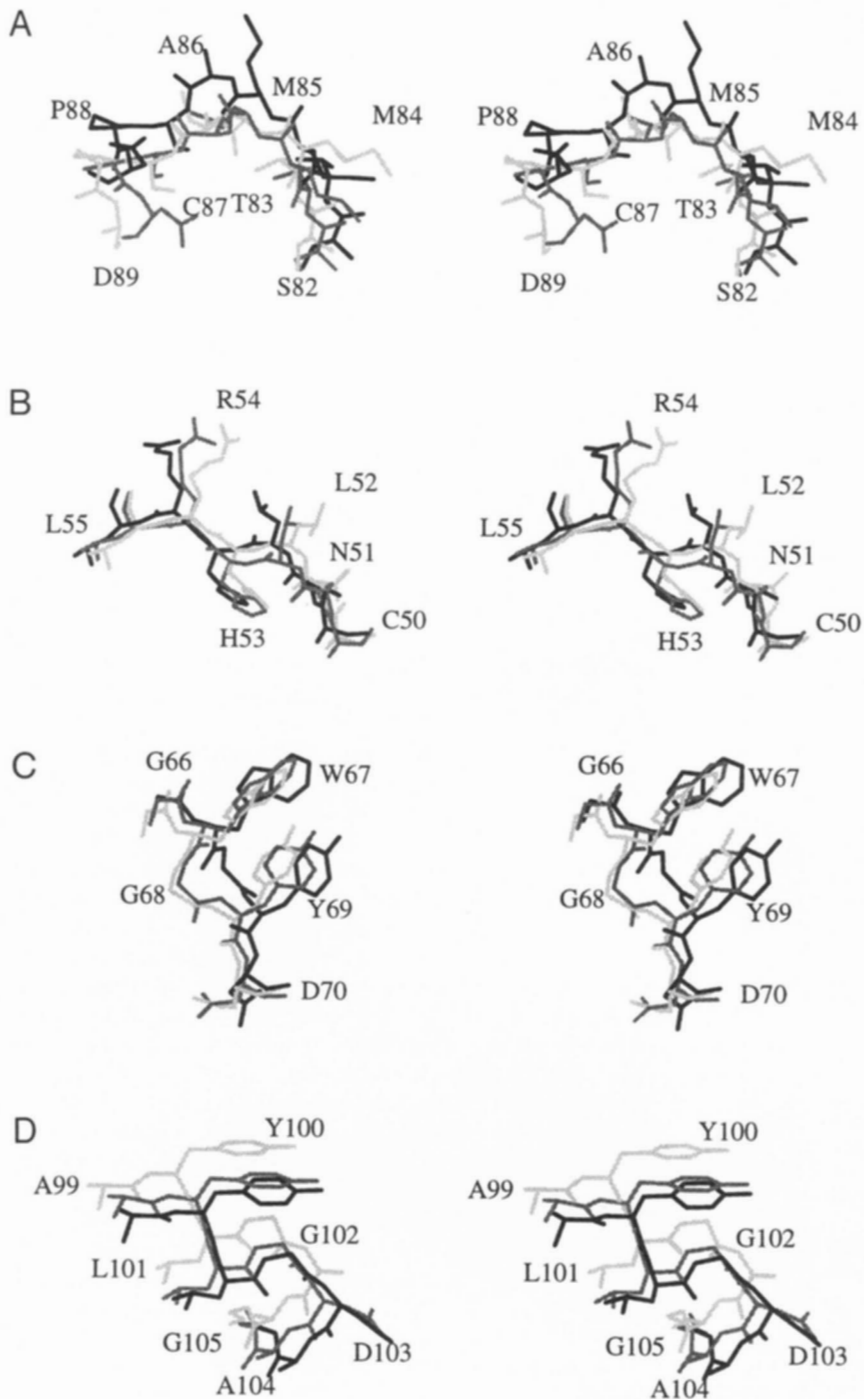


Fig. 6. Stereo diagrams comparing the regions of the inhibitor that interact with trypsin and show relatively large RMSDs among complexed (light lines), uncomplexed type I (grey lines), and uncomplexed type II (black lines) ecotin structures. **A:** Residues 82–89. **B:** Residues 50–55. **C:** Residues 66–70. **D:** Residues 99–105.

of packing is given by the fraction of atoms in a protein with zero accessible surface area. For the hyperthermophilic AOR, the fraction (~ 0.55) is significantly higher than the average (Chan et al., 1995). For uncomplexed ecotin, however, the fraction is only 0.46, not much different from the average value. Thus, the fraction of buried atoms, like surface area, does not provide a good explanation for the thermostability of ecotin. A similar case is glutamate dehydrogenase (Yip et al., 1995), for which there was no significant difference in the fraction of buried atoms between hyperthermophilic and less thermostable ones (0.62 versus 0.61). Another important factor for protein stability may be the size and number

of cavities in the structure. When the cavities in the six different triose phosphate isomerase structures were analyzed, a thermophilic enzyme from *B. stearothermophilus* had the smallest number of cavities and the smallest total cavity volume (Delboni et al., 1995). In the free ecotin structures, only a single cavity of small volume [probe-accessible volume being 19 \AA^3 and 32 \AA^3 for type I and II crystals, respectively, when calculated with probe radius 1.4 \AA using the program GRASP (Nicholls, 1992)] is present at the intersection, where the approximate molecular twofold symmetry axis passes through the dimer. This tiny cavity is formed by the aromatic rings of Trp 130 and 630. In the complexed structure of

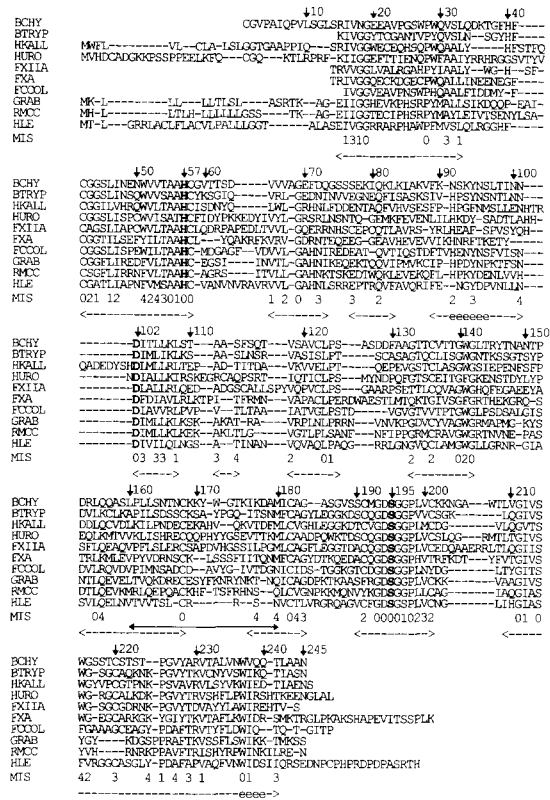


Fig. 7. Sequence alignment of ten proteases reported to be inhibited by ecotin. Sequences from National Center for Biotechnology Information protein database. The abbreviation and accession number are as follows. Bovine chymotrypsin (BCHY; KYBOA), bovine trypsin (BTRYP; S13813), human plasma kallikrein (HKALL; KQHU), human serosal urokinase (HURO; A32974), factor XIIa (FXIIA; S28941), factor Xa (FXA; A24478), fiddler crab collagenase (FCCOL; KCUF), granzyme B (GRAB; A28952), rat mast cell chymase (RMCC; S23504), and human leukocyte elastase (HLE; S06241). Catalytic triad residues in bold; e, residues interacting with secondary binding site of ecotin reported by McGrath et al. (1994). Roughly 13 homologous regions (arrows connected by dashed line) are revealed by the alignment of mammalian serine protease sequences (Greer, 1990). The region of residues approximately from 160 to 180 (chymotrypsin numbering), denoted by arrows connected by solid line, is inserted into the cleft between the primary and secondary binding sites of ecotin. The number of mismatches up to four is given below the sequence for highly conserved residues.

ecotin, this cavity is not present. Therefore, ecotin has a very tightly packed hydrophobic core and this is perhaps the most important stabilizing factor. No alanine residues are present in the hydrophobic core of ecotin and this may be correlated with its tight packing.

Another known factor for increasing protein thermostability is the stabilization of helix dipoles (Nicholson et al., 1991). However, this is irrelevant for ecotin, which lacks regular α -helices. A combination of genetic and structural studies on designed mutants of ecotin will lead to a more complete understanding of the structural origin of its exceptional thermostability.

Ecotin also shows acid stability when exposed to pH 1.0 at 4 °C for 2 h (Chung et al., 1983). The Asp-Pro bond, known to be susceptible to autolysis at acidic pH (Marcus et al., 1982), is not present in ecotin sequence. It is reasonable to assume that a complete protonation of aspartate and glutamate residues will occur at pH 1.0 and thus there will be a complete loss of ion pairs, even if

the three-dimensional structure of ecotin is assumed to be retained. It may be argued that the acid stability of ecotin partly derives from the fact that ion pairs play only a limited role in the thermostability of ecotin. In other words, even at very low pH, all major stabilizing forces in ecotin are still retained.

Materials and methods

Crystallization and X-ray data collection

The recombinant ecotin was overexpressed and purified as described previously (Lee et al., 1991a). For producing the type I crystals, the presence of 0.10% (w/v) β -octyl glucoside in the hanging drop was essential. X-ray data collection and preliminary X-ray crystallographic data for type I crystal form were reported previously (Shin et al., 1993). The crystal belongs to the space group P2₁2₁2₁ with unit cell parameters of $a = 39.22 \text{ \AA}$, $b = 84.86 \text{ \AA}$, and $c = 98.74 \text{ \AA}$. The asymmetric unit contains one dimeric molecule of ecotin, with a crystal volume per protein mass (V_m) of 2.55 $\text{\AA}^3/\text{Da}$ and a solvent content of 51.8% by volume (Matthews, 1968). Native X-ray data to 2.68 \AA were collected using the CuK α X-rays using one crystal at 18 °C.

After solving the ecotin structure in type I crystal form, a new crystal form (type II) was obtained by replacing 0.10% (w/v) β -octyl glucoside by 0.10% (w/v) trehalose. Rod crystals grew at 23 (±0.5) °C in three weeks to approximate dimensions of 0.1 mm × 0.2 mm × 0.5 mm. The native data were collected from one crystal at 14 °C using a Weissenberg camera for macromolecular crystallography at the BL-6A2 experimental station of Photon Factory, Tsukuba, Japan (Sakabe, 1991). The wavelength of synchrotron X-rays was 1.000 \AA and a 0.1-mm collimator was used. A Fuji image plate (type BAIII, 20 × 40 cm) was placed at a distance of 429.7 mm from the crystal. The oscillation range per image plate was 7.5 degrees with a speed of 2.0 degrees/s and a coupling constant of 2.0 degrees/mm. An overlap of 0.5 degree was allowed between two contiguous image plates. The diffraction patterns recorded on the image plates were digitized by a Fuji BA100 scanner. The raw data were processed using the program WEIS (Higashi, 1989). The data extended to 2.19 \AA and consisted of 67,215 measurements of 8,537 unique reflections with an R_{merge} (on intensity) of 7.3% (rejecting 3.5% outliers). The merged data set is 91.6% complete to 2.19 \AA , with the shell completeness between 2.29 \AA and 2.19 \AA being 73.2%. Refined unit cell parameters of $a = b = 63.32 \text{ \AA}$, and $c = 84.13 \text{ \AA}$ were obtained. The space group was determined to be either P4₁2₁ or its enantiomorph P4₃2₁ by inspecting the intensity distribution of the data. The latter space group was found to be correct on the basis of later translation function calculations. There is one monomer in the asymmetric unit ($V_m = 2.62 \text{ \AA}^3/\text{Da}$; solvent content = 53.1%) (Matthews, 1968).

Molecular replacement

The program X-PLOR (Brünger, 1992) was used for the molecular replacement calculation. Reflections with $F_o > 2 \sigma F$ were used throughout the molecular replacement and subsequent refinement calculations. In solving the ecotin structure of type I crystal, the search model was the model of the dimeric inhibitor in the previously reported structure of ecotin-trypsin complex (McGrath et al., 1994) (the refined complex model has an R -factor of 18.0% for the 6–2.4 \AA data, with RMSD from ideal stereochemistry of

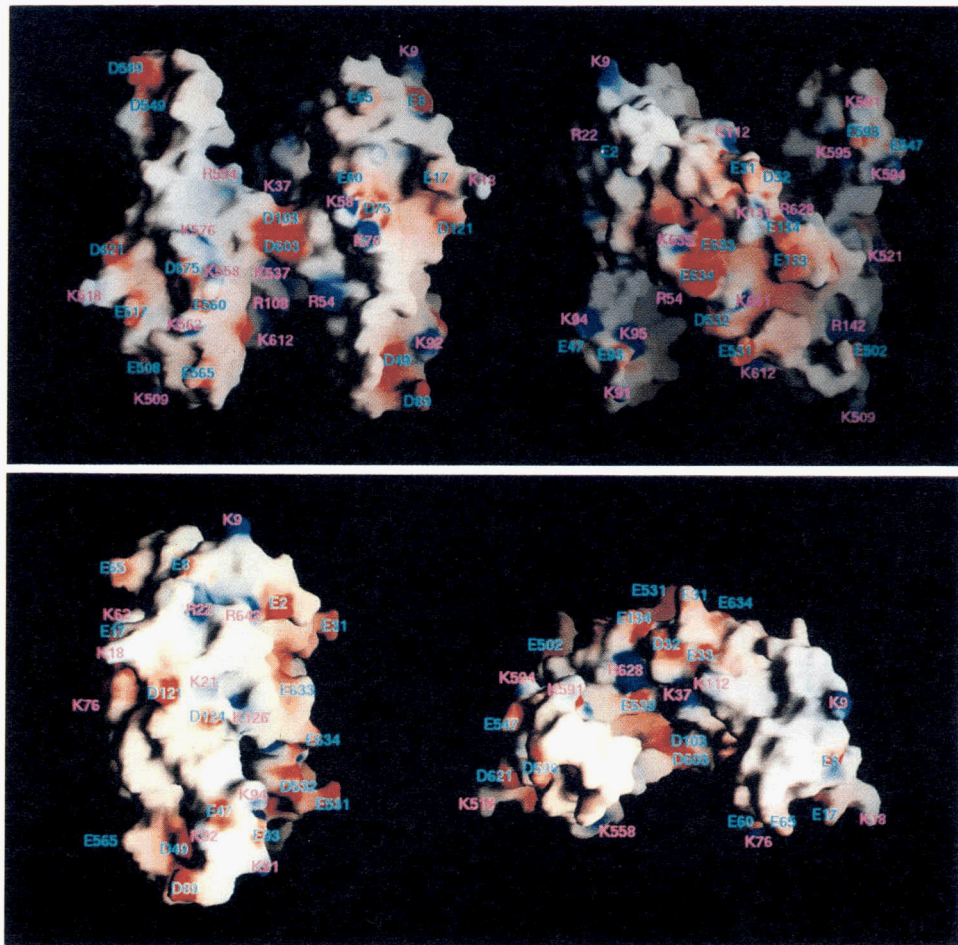


Fig. 8. Molecular surface of uncomplexed ecotin (in orthorhombic, type I crystal) colored according to electrostatic potential. Positively charged regions are blue and negatively charged regions red. Top: when the view on the left side is rotated by 180 degrees around the vertical axis, the view on the right is obtained. Bottom: the left view is from the side and the right view is from the top. Figures were generated using GRASP (Nicholls, 1992).

0.10 Å and 2.85 degrees for bond distances and angles, respectively). In the starting model, six residues, 1–4 and 90–91, were missing from each subunit and eight residues (5, 9, 58, 65, 89, 92, 93, 103) were modeled as alanines. The two subunits, related by a noncrystallographic twofold symmetry, agreed with RMSDs of 0.66 Å and 0.79 Å for main-chain and side-chain atoms, respectively. The probe structure factors were calculated by placing the starting model in an orthogonal unit cell with dimensions of 100 Å × 100 Å × 100 Å. The orientations were sampled by using the pseudo-orthogonal Eulerian angles. The rotation function search was conducted using a maximum Patterson radius of 30 Å and a step size of 2.5 Å. A clear solution was obtained only when the low-resolution data down to 20.0 Å were included. Rigid-body Patterson correlation refinement (PC refinement) was then performed on 89 orientations produced by the above cross rotation search for the 20.0–3.5-Å data. The PC refinement gave a clear rotation function solution: $\alpha = 259.8$ degrees, $\beta = 91.7$ degrees, and $\gamma = 161.0$ degrees. Next, the translation function, calculated using the 20.0–3.5-Å data, yielded the translation solution as $x = 0.450$, $y = 0.460$, and $z = 0.325$ in fractional coordinates. One dimer in the asymmetric unit, after being oriented and positioned according to the above solution, gave an *R*-factor of 51.1% for the 8.0–3.5 Å data.

For the type II crystal form, the starting model for the molecular replacement calculation was a single subunit in the model of ecotin in type I crystal, which was refined to an *R*-factor of 18.0% for the 6.0–2.68-Å data with RMSD from ideal stereochemistry of 0.009 Å and 1.55 degrees for bond distances and angles, respectively. Each subunit in the unrotated ecotin model failed to give a clear solution for the cross rotation function. Therefore, the calculation was repeated after rotating the starting model by Eulerian angles of $\theta_1 = 22.0$ degrees, $\theta_2 = 33.0$ degrees, and $\theta_3 = 44.0$ degrees. This gave a clear solution: $\alpha = 288.8$ degrees, $\beta = 58.9$ degrees, and $\gamma = 245.9$ degrees. Next, the translation function was calculated using the 20.0–3.5-Å data to obtain the translation solution: $x = 0.207$, $y = 0.262$, $z = 0.000$ in fractional coordinates. A single monomer in the asymmetric unit, after being oriented and positioned according to the above solution, gave an *R*-factor of 43.6% for the 8.0–3.5-Å data.

Refinement

The program X-PLOR (Brünger, 1992) was used for all refinement calculations. Only reflections with $F_o > 2\sigma F$ were included throughout the refinement calculations. Isotropic *B*-factors for individual atoms were fixed initially to 15 Å² and were refined in the last

stages. For the type I crystal, the noncrystallographic symmetry restraint between the two subunits was relaxed only at the final stage of the refinement. The $2F_o - F_c$ and $F_o - F_c$ maps were used for the manual rebuilding between refinement cycles and for the location of solvent and additive molecules. When the refined *B*-factor of a solvent molecule exceeded 80 Å², it was removed.

For the type I crystal, an initial rigid-body refinement was started with the 8.0–6.0-Å data to further improve the positional and orientational parameters. The higher-resolution data were added in steps to 3.5 Å, as the number of rigid bodies was increased from 2 to 14. The *R*-factor at this stage was 43.8% for the 8.0–3.5-Å data. Next, atomic positions were refined by the conventional conjugate gradient minimization, with high-resolution data being added in steps. The model was then subject to the simulated annealing refinement, employing the standard slow cooling protocol from 4,000 K to 300 K (time-step 0.5 fs; decrement of temperature 25 K; number of steps at each temperature 50). Missing residues (1–4, 90–91), as well as the residues modeled as alanines in the starting model, were built with correct residues during several conventional positional refinement cycles, with the *R*-factor dropping to 26.8% for the 6.0–2.68-Å data. The $2F_o - F_c$ and $F_o - F_c$ electron density maps revealed the bound β-octyl glucoside molecules and a total of 21 could be located in the asymmetric unit. After positional refinement, the *R*-factor dropped to 25.2% for the same data. Water molecules were added to the model and the noncrystallographic symmetry restraint between the two independent subunits in the asymmetric unit were relaxed. At this stage, the *R*-factor dropped to 23.8%. Finally, the refinement of isotropic *B*-factors for individual atoms, initially fixed to 15 Å², gave the final *R*-factor of 18.0% for the 6.0–2.68-Å data.

For the type II crystal, a total of 18 trehalose molecules could be located in the asymmetric unit after the simulated annealing refinement. The *R*-factor was reduced to 28.0% for the 6.0–2.19-Å data during conventional positional refinement steps. After adding water molecules and refining isotropic *B*-factors for individual atoms in the final cycle, the *R*-factor dropped to 21.3% for the 6.0–2.19-Å data.

Model building and structure analysis

For the model rebuilding and the display of electron density maps, the graphics programs FRODO (Jones, 1985), running on an Evans & Sutherland PS390 graphics system, and CHAIN (Sack, 1988), running on a Silicon Graphics Indigo2 XZ workstation, were used. At each stage of the model rebuilding and refinement, the stereochemistry of the model was assessed by the program PROCHECK (Laskowski et al., 1993). Structural comparisons were made using the program LSQKAB in CCP4 program package (CCP4, 1994).

Structure coordinates

The atomic coordinates and structure factor data have been deposited in the Brookhaven Protein Data Bank (PDB ID: 1ECZ, R1ECZSF for type I crystal and 1ECY, R1ECYSF for type II crystal).

Acknowledgments

We thank the Inter-University Center for Natural Science Research Facilities for providing the X-ray equipment. This work was supported by a Basic Sciences Research Institute grant from the Ministry of Education, Center for Molecular Catalysis, Korea Science and Engineering Foundation (95-0501-07-01-3), and Research Center for Cell Differentiation (C.H.C.). We thank Prof. R.J. Fletterick and Dr. M.E. McGrath for pro-

viding the coordinates of ecotin. We also thank Prof. N. Sakabe, Dr. A. Nakagawa, and Dr. N. Watanabe for assistance during data collection at BL-6A2 of Photon Factory, Japan.

References

- Ahern TJ, Klibanov AM. 1985. The mechanism of irreversible enzyme inactivation at 100°C. *Science* 228:1280–1284.
- Aswad DW. 1990. Formation of isoaspartate in human growth hormone and bovine brain calmodulin. *Enzyme Eng* 10:26–36.
- Barlow DJ, Thornton JM. 1983. Ion pairs in proteins. *J Mol Biol* 168:867–885.
- Bennett MJ, Schlunegger MP, Eisenberg D. 1995. 3D domain swapping: A mechanism for oligomer assembly. *Protein Sci* 4:2455–2468.
- Blevins RA, Tulinsky A. 1985. The refinement and the structure of the dimer of α-chymotrypsin at 1.67-Å resolution. *J Biol Chem* 260:4264–4275.
- Bode W, Chen Z, Bartels K, Kutzbach C, Schmidt-Kastner G, Bartunk H. 1983. Refined 2 Å X-ray crystal structure of porcine pancreatic kallikrein A, a specific trypsin-like serine proteinase. Crystallization, structure determination, crystallographic refinement, structure and its comparison with bovine trypsin. *J Mol Biol* 164:237–282.
- Bode W, Huber R. 1991. Ligand binding: Proteinase–protein inhibitor interactions. *Curr Opin Struct Biol* 1:45–52.
- Bode W, Huber R. 1992. Natural protein proteinase inhibitors and their interaction with proteinases. *Eur J Biochem* 204:433–451.
- Bode W, Schwager P. 1975. The refined crystal structure of bovine β-trypsin at 1.8 Å resolution. II. Crystallographic refinement, calcium binding site, benzamidine binding site and active site at pH 7.0. *J Mol Biol* 98:693–717.
- Bode W, Wei AZ, Huber R, Meyer E, Travis J, Neumann S. 1986. X-ray crystal structure of human leukocyte elastase (PMN elastase) and the third domain of turkey ovomucoid inhibitor. *EMBO J* 5:2453–2458.
- Brünger AT. 1992. *X-PLOR manual version 3.1: A system for X-ray crystallography and NMR*. New Haven, Connecticut: Yale University.
- CCP4. 1994. Collaborative Computational Project Number 4. The CCP4 suite: Programs for protein crystallography. *Acta Crystallogr D* 50:760–763.
- Chan MK, Mukund S, Kletzin A, Adams MWW, Rees DC. 1995. Structure of a hyperthermophilic tungstate oxygen enzyme, aldehyde ferredoxin oxidoreductase. *Science* 267:1463–1469.
- Chung CH, Ives HE, Almeda S, Goldberg AL. 1983. Purification from *Escherichia coli* of a periplasmic protein that is a potent inhibitor of pancreatic proteases. *J Biol Chem* 258:11032–11038.
- Delboni LF, Mande SC, Rentier-Delrue F, Mainfray V, Turley S, Vellieux FMD, Martial JA, Hol WGJ. 1995. Crystal structure of recombinant triosephosphate isomerase from *Bacillus stearothermophilus*. An analysis of potential thermostability factors in six isomerases with known three-dimensional structures points to the importance of hydrophobic interactions. *Protein Sci* 4:2594–2604.
- Eom SH, Song HK, Suh SW, Kim Y, Steitz TA, Park JH, Kim JS, Kwon ST, Lee DS. 1995. Crystallization and preliminary X-ray crystallographic analysis of DNA polymerase from *Thermus aquaticus*. *Acta Crystallogr D* 51:1086–1088.
- Fujinaga M, James MNG. 1987. Rat submaxillary gland serine protease, tonin: Structure solution and refinement at 1.8 Å resolution. *J Mol Biol* 195:373–396.
- Greer J. 1990. Comparative modeling methods: Application to the family of the mammalian serine proteases. *Protein Strut Funct Genet* 7:317–334.
- Henning M, Darimont B, Stern R, Kirschner K, Janssonius J. 1995. 2.0 Å structure of indole-3-glycerol phosphate synthase from the hyperthermophile *Sulfolobus solfataricus*: Possible determinants of protein stability. *Structure* 3:1295–1306.
- Higashi T. 1989. The processing of diffraction data taken on a screenless Weissenberg camera for macromolecular crystallography. *J Appl Crystallogr* 22:9–18.
- Jones TA. 1985. Interactive computer graphics: FRODO. *Methods Enzymol* 115:157–171.
- Kojima S, Kumagai I, Miura K. 1993. Requirement for a disulfide bridge near the reactive site of protease inhibitor SSI (*Streptomyces* subtilisin inhibitor) for its inhibitory action. *J Mol Biol* 230:395–399.
- Kraulis PJ. 1991. MOLSCRIPT: A program to produce both detailed and schematic plots of protein structures. *J Appl Crystallogr* 24:946–950.
- Laskowski RA, MacArthur MW, Moss DS, Thornton JM. 1993. PROCHECK: A program to check the stereochemical quality of protein structures. *J Appl Crystallogr* 26:283–291.
- Lee HR, Seol JH, Kim OM, Lee CS, Suh SW, Hong YM, Tanaka K, Ichihara A, Ha DB, Chung CH. 1991a. Molecular cloning of the ecotin gene in *Escherichia coli*. *FEBS Lett* 287:53–56.
- Lee SY, Kim S, Sweet RM, Suh SW. 1991b. Crystallization and a preliminary X-ray crystallographic study of α-amylase from *Bacillus licheniformis*. *Arch Biochem Biophys* 291:255–257.

- Luzzati V. 1952. Traitement statistique des erreurs dans la détermination des structures cristallines. *Acta Crystallogr* 5:802–810.
- Marcus F, Edelstein I, Reardon I, Heinrikson RL. 1982. Complete amino acid sequence of pig kidney fructose-1,6-bisphosphatase. *Proc Natl Acad Sci USA* 79:7161–7165.
- Marks CB, Naderi H, Kosen PA, Kuntz ID, Anderson S. 1987. Mutants of bovine pancreatic trypsin inhibitor lacking cysteines 14 and 38 can fold properly. *Science* 235:1370–1373.
- Matthews BW. 1968. Solvent content of protein crystals. *J Mol Biol* 33:491–497.
- McGrath ME, Erpel T, Browner MF, Fletterick RJ. 1991a. Expression of the protease inhibitor ecotin and its co-crystallization with trypsin. *J Mol Biol* 222:139–142.
- McGrath ME, Erpel T, Bystoff C, Fletterick RJ. 1994. Macromolecular chelation as an improved mechanism of protease inhibition: Structure of the ecotin–trypsin complex. *EMBO J* 13:1502–1507.
- McGrath ME, Gillmor SA, Fletterick RJ. 1995. Ecotin: Lessons on survival in protease-filled world. *Protein Sci* 4:141–148.
- McGrath ME, Hines WM, Sakanari JA, Fletterick RJ, Craik CS. 1991b. The sequence and reactive site of ecotin: A general inhibitor of pancreatic serine proteases from *Escherichia coli*. *J Biol Chem* 266:6620–6625.
- McPherson A, Koszelak S, Axelrod H, Day J, Williams R, Robinson L, McGrath M, Cascio D. 1986. An experiment regarding crystallization of soluble proteins in the presence of β -octyl glucoside. *J Biol Chem* 261:1969–1975.
- Narayana SVL, Carson M, El-Kabbani O, Kilpatrick JM, Moore D, Chen X, Bugg CE, Volanakis JE, DeLucas LJ. 1994. Structure of human factor D; a complement system protein at 2.0 Å resolution. *J Mol Biol* 235:695–708.
- Nicholls A. 1992. GRASP: Graphical representation and analysis of surface properties. New York: Columbia University.
- Nicholson H, Anderson DE, Dao-pin S, Matthew BW. 1991. Analysis of the interaction between charged side chains and the α -helix dipole using designed thermostable mutants of phage T4 lysozyme. *Biochemistry* 30:9816–9828.
- Padmanabhan K, Padmanabhan KP, Tulinsky A, Park CH, Bode W, Huber R, Blankenship DT, Cardin AD, Kisiel W. 1993. Structure of human des(1–45) factor Xa at 2.2 Å resolution. *J Mol Biol* 232:947–966.
- Perona JJ, Tsu CA, Craik CS, Fletterick RJ. 1993a. Crystal structures of rat anionic trypsin complexed with the protein inhibitors APPI and BPTI. *J Mol Biol* 230:919–933.
- Perona JJ, Tsu CA, McGrath ME, Craik CS, Fletterick RJ. 1993b. Relocating a negative charge in the binding pocket of trypsin. *J Mol Biol* 230:934–949.
- Politz O, Simon O, Olsen O, Borrius R. 1993. Determinants for the enhanced thermostability of hybrid (1-3,1-4)- β -glucanases. *Eur J Biochem* 216:829–834.
- Read RJ, James MNG. 1988. Refined crystal structure of *Streptomyces griseus* trypsin at 1.7 Å resolution. *J Mol Biol* 200:523–551.
- Remington SJ, Woodbury RG, Reynolds RA, Matthews BW, Neurath H. 1988. The structure of rat mast cell protease II at 1.9-Å resolution. *Biochemistry* 27:8097–8105.
- Russell RJM, Hough DW, Danson MJ, Taylor GL. 1994. The crystal structure of citrate synthase from the thermophilic archaeon, *Thermoplasma acidophilum*. *Structure* 2:1157–1167.
- Sack JS. 1988. CHAIN—A crystallographic modeling program. *J Mol Graphics* 6:244–245.
- Sakabe N. 1991. X-ray diffraction data collection system for modern protein crystallography with a Weissenberg camera and an imaging plate using synchrotron radiation. *Nucl Instrum Meths A* 303:448–463.
- Schreuder HA, de Boer B, Dijkema R, Mulders J, Theunissen HJM, Grootenhuis PDJ, Hol WJG. 1994. The intact and cleaved human antithrombin III complex as a model for serpin–proteinase interactions. *Nature Struct Biol* 1:48–54.
- Seong IS, Lee HR, Seol JH, Park SK, Lee CS, Suh SW, Hong YM, Kang MS, Ha DB, Chung CH. 1994. The P₁ reactive site methionine residue of ecotin is not crucial for its specificity on target proteases. *J Biol Chem* 269:21915–21918.
- Seymour JL, Lindquist RN, Dennis MS, Moffat B, Yansura D, Reilly D, Wessinger ME, Lazarus RA. 1994. Ecotin is a potent anticoagulant and reversible tight-binding inhibitor of factor Xa. *Biochemistry* 33:3949–3958.
- Shin DH, Hwang KY, Kim KK, Lee HR, Lee CS, Chung CH, Suh SW. 1993. Crystallization and preliminary X-ray crystallographic analysis of the protease inhibitor ecotin. *J Mol Biol* 229:1157–1158.
- Song HK, Lee KN, Kwon KS, Yu MH, Suh SW. 1995. Crystal structure of an uncleaved α_1 -antitrypsin reveals the conformation of its inhibitory reactive loop. *FEBS Lett* 377:150–154.
- Takeuchi Y, Satow Y, Nakamura KT, Mitsui Y. 1991. Refined crystal structure of the complex of subtilisin BPN' and *Streptomyces* subtilisin inhibitor at 1.8 Å resolution. *J Mol Biol* 221:309–325.
- Tsu CA, Perona JJ, Schellenberger V, Turck CW, Craik CS. 1994. The substrate specificity of *Uca pugilator* collagenolytic serine protease 1 correlates with the bovine type I collagen cleavage sites. *J Biol Chem* 269:19565–19572.
- Ulmer JS, Lindquist RN, Dennis MS, Lazarus RA. 1995. Ecotin is a potent inhibitor of the contact system proteases factor XIIa and plasma kallikrein. *FEBS Lett* 365:159–163.
- Yip KSP, Stillman TJ, Britton KL, Artymuik PI, Baker PJ, Sedelnikova SE, Engel PC, Pasquo A, Chiaraluce R, Consalvi V, Scandurra R, Rice DW. 1995. The structure of *Pyrococcus furiosus* glutamate dehydrogenase reveals a key role for ion pair networks in maintaining enzyme stability at extreme temperatures. *Structure* 3:1147–1158.